

Stratospheric Variability in Twentieth-Century CMIP5 Simulations of the Met Office Climate Model: High Top versus Low Top

SCOTT M. OSPREY AND LESLEY J. GRAY

National Centre for Atmospheric Science, University of Oxford, Oxford, United Kingdom

STEVEN C. HARDIMAN, NEAL BUTCHART, AND TIM J. HINTON

Met Office Hadley Centre, Exeter, United Kingdom

(Manuscript received 6 March 2012, in final form 8 August 2012)

ABSTRACT

An examination is made of stratospheric climate, circulation, and variability in configurations of the Hadley Centre Global Environmental Model version 2 (HadGEM2) differing only in stratospheric resolution and the placement of the model lid. This is made in the context of historical reconstructions of twentieth-century climate. A reduction in the westerly bias in the Northern Hemisphere polar night jet is found in the high-top model. The authors also find significant differences in the expression of tropical stratospheric variability, finding improvements in the high-top model for the presence of the quasi-biennial oscillation, for tropical upwelling consistent with interim European Centre for Medium-Range Weather Forecasts (ECMWF) Re-Analysis (ERA-Interim) data, and for interannual changes in stratospheric water vapor concentration comparable to satellite observations. Further differences are seen at high latitudes during winter in the frequency of occurrence of sudden stratospheric warmings (SSWs). The occurrence rate of SSWs in the high-top simulations, $(7.2 \pm 0.5) \text{ decade}^{-1}$, is statistically consistent with observations, $(6.0 \pm 1.0) \text{ decade}^{-1}$, whereas they are one-third as frequent in the low-top simulations, $(2.5 \pm 0.5) \text{ decade}^{-1}$. Furthermore, the structure of the timing of winter final warmings is only captured in the high-top model. A similar characterization for the time evolution of the width of the tropical upper troposphere is found between model configurations. It is concluded that an adequate representation of the stratosphere is required to capture the important modes of tropical and extratropical stratospheric variability in models.

1. Introduction

Reconstructions of past climate are not only necessary for validating key processes in models, they are also important in the understanding of how key processes may be affected by future climate change. In particular, model reconstructions of past climate are valuable for examining those parts of the climate system poorly sampled by observations, one example being stratospheric climate and variability prior to global satellite observations and their subsequent assimilation into reanalyses such as the 40-yr European Centre for Medium-Range Weather Forecasts (ECMWF) Re-Analysis (ERA-40; Uppala et al. 2005).

The inclusion of a well-resolved stratosphere in global climate models is thought to be important for an adequate

representation of troposphere–stratosphere covariance and for improvements in the skill of short-term seasonal weather prediction (Maycock et al. 2011; Shaw and Shepherd 2008; Baldwin et al. 2003; Baldwin and Dunkerton 2001). Furthermore, idealized modeling studies have identified a sensitivity of the large-scale tropospheric circulation to imposed changes to the state and variability of the stratosphere (Woollings et al. 2010b; Ineson and Scaife 2009; Bell et al. 2009; Scaife et al. 2005; Norton 2003). But how well resolved does the stratosphere need to be to better capture the variability relevant to weather regimes in the troposphere? Or how well resolved does the stratosphere need to be to better capture the observed stratospheric climate and variability?

Recent modeling studies have sought to address the first question and have found a sensitivity of the tropospheric circulation to specification of orographic gravity wave drag (Sigmond et al. 2008), unphysical effects following wave reflection near the model lid in low-top

Corresponding author address: Scott Osprey, Clarendon Laboratory, University of Oxford, Oxford OX1 3PU, United Kingdom.
E-mail: s.osprey@physics.ox.ac.uk

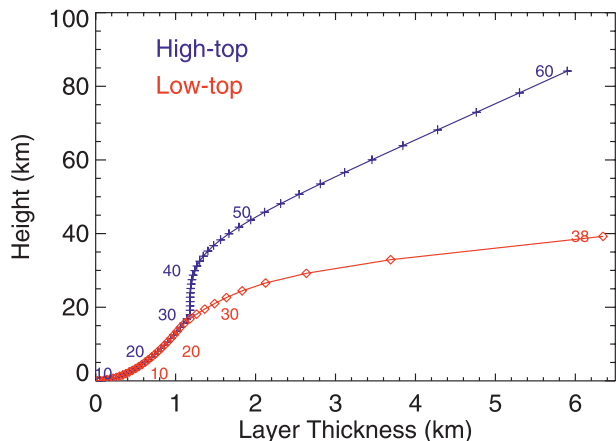


FIG. 1. Distribution of model level and thickness within the low-top and high-top configurations of HadGEM2-CC. The numbers denote the placement of model levels. Note the common placement of levels below ~ 16 km.

models (Sassi et al. 2010), and changes in tropospheric circulation, including significant warming of the near-surface Arctic, following a realistic prescription of stratospheric ozone and tropical variability in a low-top model (Dall'Amico et al. 2010). Other studies provide varying support of stratospheric impacts on tropospheric variability, notably concerning future projections of the mean position of the North Atlantic storm track (Scaife et al. 2012) and tropospheric blocking (Woollings et al. 2010a; Martius et al. 2009; Taguchi 2008; Quiroz 1986).

We seek to partially address the second question, using two configurations of the Hadley Centre Global Environmental Model version 2 (HadGEM2), differing only in the placement of the model lid and vertical resolution above 16 km. Examination of other factors thought important to stratospheric climate and variability, such as prescriptions of atmospheric composition, chemistry, and parameterizations (e.g., gravity waves), are outside the scope of this paper. This present study is set in the context of a historical reconstruction of twentieth-century climate.

2. Methods

For this study we compare the performance of two model configurations of the Met Office global climate model running with an interactive carbon cycle (CC). We refer to the version with 38 vertical levels and a height of the model lid at 39 km as the *low top* (HadGEM2-CC), while the more stratosphere-resolving *high-top* configuration (HadGEM2-CCS) has a total of 60 levels in the vertical and a model lid at 84 km (Fig. 1). Both models are part of the family of Met Office model configurations known collectively as HadGEM2 (Martin et al. 2011).

In this study, the low-top configuration not only employs the same forcings as those used in the high top, the included physics packages and their respective settings are the same. Physical parameterizations relevant to the stratosphere include the parameterized effects of orographic gravity waves together with a treatment of the propagation and dissipation of a prescribed broad spectrum of gravity waves (Scaife et al. 2002). Other notable parameterizations include the production of stratospheric water vapor from methane oxidation (Simmons et al. 1999) and longwave radiative transfer in the upper stratosphere and mesosphere (Zhong and Haigh 2000). No allowance is made for systematic differences in downwelling radiance between the low-top and high-top models near the uppermost level of the low-top model. Further details of other included physics packages are outlined in Martin et al. (2011).

As described in Hardiman et al. (2012), ensembles of historical simulations are compiled for low top and high top: one member over the extended period of 1860–2006 and two further covering the recent past (1960–2005). Initial condition data for the extended runs are compiled from centuries-long control integrations with stationary external forcings. Time-varying forcings are as outlined for the Coupled Model Intercomparison Project Phase 5 (CMIP5; <http://cmip-pcmdi.llnl.gov/cmip5>), the details of which are described in Jones et al. (2011). For this study we use a modified version of the Stratospheric Processes and their Role in Climate (SPARC) ozone dataset described by Cionni et al. (2011). The modifications include a vertical extrapolation of the ozone data above 1 hPa to coincide with the upper levels in the high-top configuration and the representation of a solar cycle at high latitudes.

Specifically, the SPARC ozone number density time series, originally based on a multiple linear regression analysis, was separated into time-dependent components identified with solar forcing (O_3^{sol}), equivalent effective stratospheric chlorine (O_3^{Cl}), a seasonal cycle (O_3^{seas}), and a residual term (O_3^{res}):

$$O_3(t) = \alpha O_3^{\text{sol}} + \beta O_3^{\text{Cl}} + O_3^{\text{seas}} + O_3^{\text{res}}. \quad (1)$$

The last two terms (which also represent climatology) are extrapolated above 1 hPa according to

$$O_3(z) = O_3(z_1) \exp[(z_1 - z)/H], \quad (2)$$

where z_1 is the highest level in the original SPARC dataset and H represents a scale height of 7 km. The coefficients for solar forcing α and equivalent effective stratospheric chlorine β are strongly reduced in height (scale height of 3.5 km) to reduce the presence of unobserved stratospheric trends and variability in the mesospheric ozone,

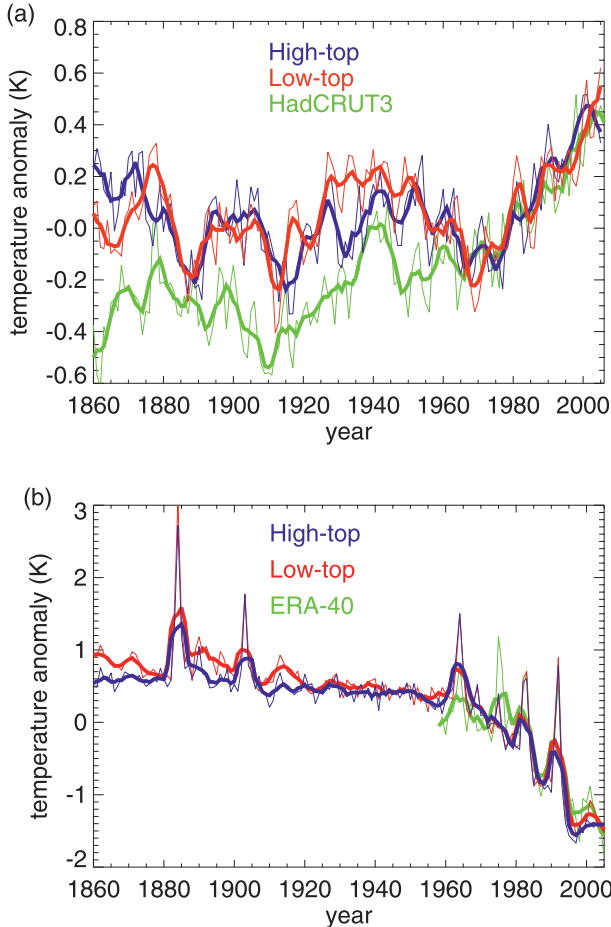


FIG. 2. Global annual mean (a) 1.5-m and (b) 50-hPa temperature anomalies (K) for the 1860–2005 low-top and high-top historical simulations, HadCRUT3 observations, and ERA-40. A 5-yr smoothing is shown in bold and anomalies are with respect to the 1961–90 mean.

which would arise from the extrapolation of ozone above 1 hPa. A cosine-latitude extrapolation of the solar term is made over high latitudes to better account for an unrealistic lack of solar variability in the original SPARC dataset.

The remainder of the paper is laid out as follows: we assess the near-surface temperature trends and variability in low-top and high-top ensembles before examining the mean climate of the stratosphere. We showcase tropical stratospheric variability using examples of the quasi-biennial oscillation (QBO), upwelling, the tropical tape recorder in water vapor (TTR), and the width in latitude of the tropical upper troposphere. We then select the age of air, the frequency of SSWs, and finally the timing of final warmings as being the key features of variability in the extratropical stratosphere. Unless otherwise stated, we use ensemble averages and compare

against ERA-40 and ERA-Interim data (Uppala et al. 2005; Dee et al. 2011), and significance testing is done using the Student's *t* test.

3. Results

a. Climatology and time series

Figure 2 shows changes in global annual mean near-surface temperature anomalies over the historical period, 1860–2006. The reference period used is 1961–90 as recommended by Solomon et al. (2007). The range in surface temperature shown in both low-top and high-top models is around 0.8 K, which compares to approximately 1.0 K as seen in the HadCRUT3 observations (Brohan et al. 2006; Jones et al. 1999; Rayner et al. 2006, 2003). Both model configurations show an increase in global surface temperature from 1970 onward and the same rate of warming (0.25 ± 0.10) K decade $^{-1}$. Prior to this period, considerable decadal variability is evident and is comparable in magnitude to recent changes observed post-1970 and predicted from other studies (Cox et al. 2000). A decrease in global surface temperature during the period 1940–70 is reproduced in both low- and high-top model simulations. A similar, though larger, decrease in the positive temperature trends is seen in the HadCRUT3 observations and has been described elsewhere (Jones and Moberg 2003; Brohan et al. 2006; Jones et al. 1999). This is consistent with aerosol-induced negative radiative forcing cited in previous studies (Mitchell et al. 1995; Roeckner et al. 1999; Stott et al. 2000).

Global annual mean 50-hPa temperature anomalies for the low-top and high-top simulations over the historical period are shown in Fig. 2b. Once more, the reference period is defined as the 1961–90 average. The effects following changes in ozone concentrations are clearly seen post-1960. The trend is for decreasing global temperatures and is a consequence of reduced shortwave heating from decreasing ozone concentrations (D. Mitchell 2012, personal communication). The response following past volcanic eruptions is also apparent as periods of brief yet strong changes in global stratospheric temperature. The downward trend in global 50-hPa temperature levels off after 1995. This result has been extensively reported in other studies [see Seidel et al. (2011) for a review]. In the low-top and high-top ensembles, this is attributed to stratospheric ozone and aerosol effects (D. Mitchell 2012, personal communication).

Figure 3 shows latitude–height sections of zonal mean temperature during December–February (DJF) and June–August (JJA) for the low-top and high-top ensembles. The DJF comparisons cover the period 1958–2006

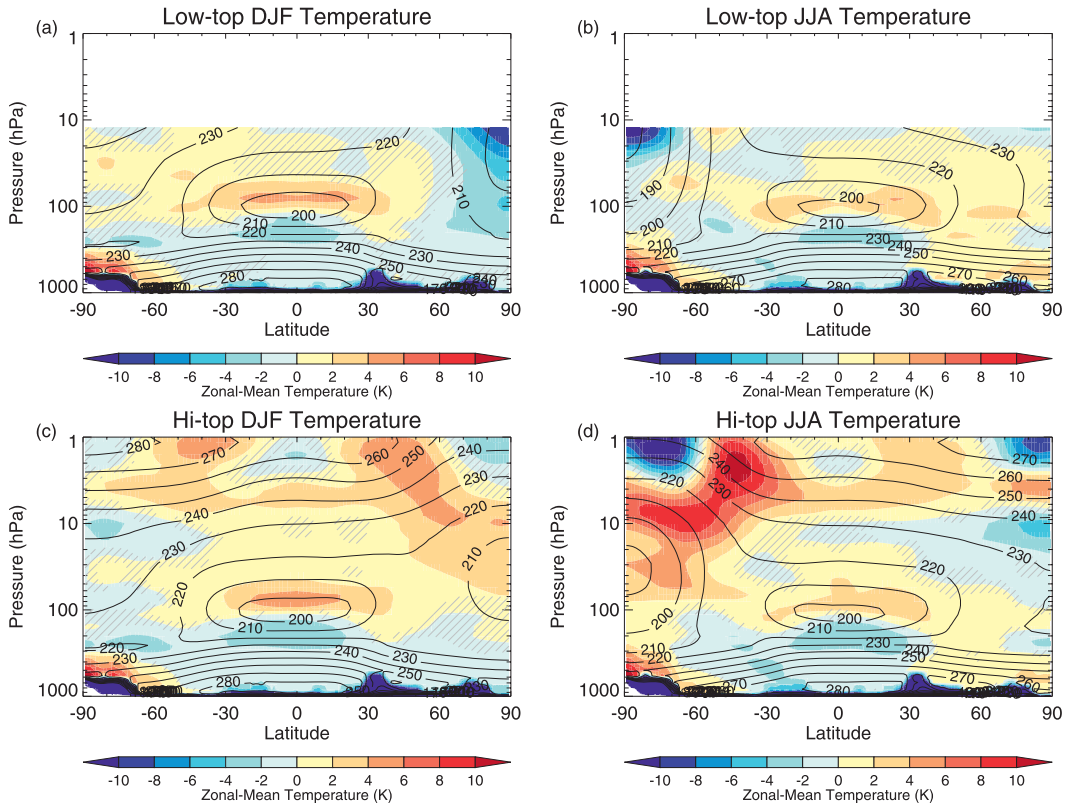


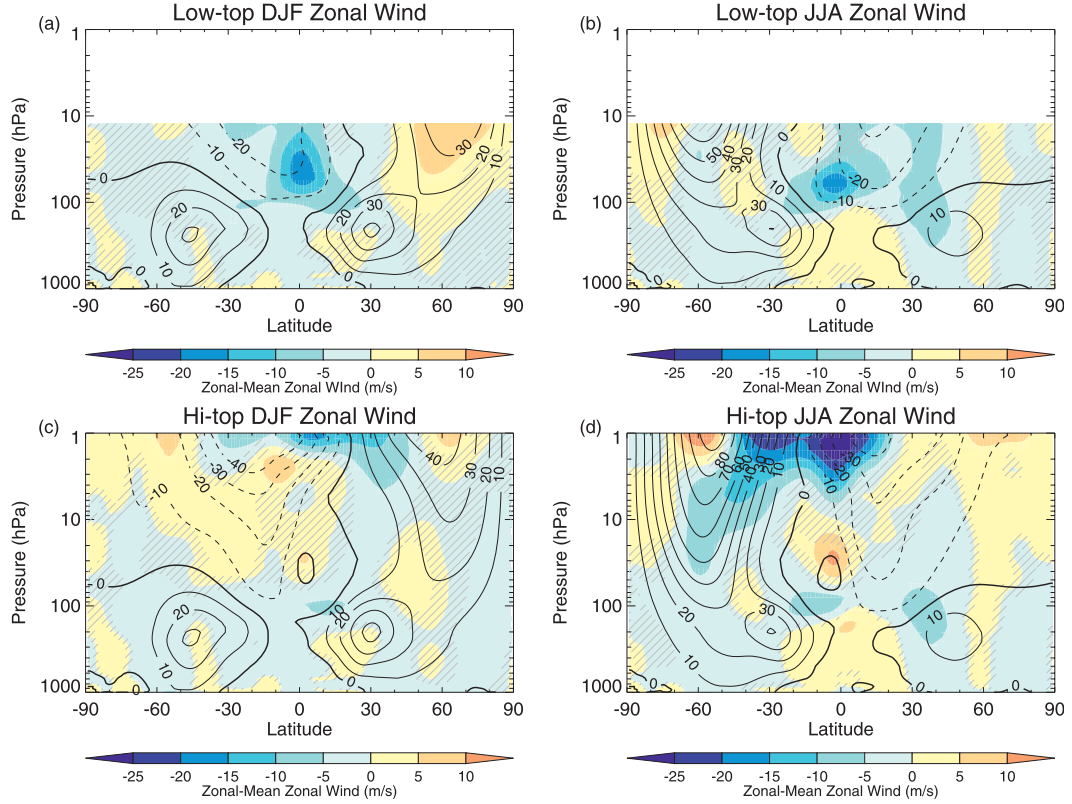
FIG. 3. Height-latitude temperature anomalies (K) for the (a),(b) low-top and (c),(d) high-top ensembles during (a),(c) DJF and (b),(d) JJA, respectively. DJF anomalies are with respect to ERA-40 from 1958 to 2002 and ERA-Interim from 2002 onward, while the period for comparison for JJA is chosen to be 1979–2006. Overlaid (line contours) are ensemble-mean values and unshaded regions denote significant differences at the 95% level.

to coincide with coverage from ERA-40 and ERA-Interim. Both low-top and high-top ensembles exhibit weak cold biases in the troposphere and warm biases in the stratosphere, compared to the reanalyses. Furthermore, the tropical tropopause is warmer in both models and geometrically lower in the high top (not shown), compared to reanalyses. In DJF, differences between the simulations can be seen at northern high latitudes in the stratosphere, where the cold bias in the low-top simulation (-10 K) is replaced with a weak warm bias in the high-top simulation ($2\text{--}4\text{ K}$). This is consistent with increased planetary wave driving in the high-top simulation (not shown).

The period for comparison for JJA is chosen to be 1979–2006 to reflect better observational data coverage over the Southern Hemisphere at these times. Zonal mean temperatures during JJA exhibit similar biases with respect to the reanalyses. The warm bias, as compared with the reanalyses, in tropical tropopause temperature is reduced compared with DJF, though it peaks at lower pressure. Considerable differences are found between the low- and high-top simulations throughout

the southern high-latitude stratosphere. Weak cold biases in the low-top simulations are replaced by strong warm biases in the high-top ones. Peak biases in the low stratosphere are around $4\text{--}6\text{ K}$, which would be relevant in modeling ozone chemistry. Above 10 hPa , differences in the height of the southern polar stratopause between the high-top simulations and the reanalyses show up as a strong dipole feature. Reanalysis temperatures at these altitudes are less reliable than elsewhere because of the paucity of observations being assimilated, so these differences are less likely to be significant.

Seasonal distributions for zonal mean zonal wind can be seen in Fig. 4. A comparison of stratospheric wind during DJF shows a reduction in bias from the low- to high-top model at midlatitudes. This is directly linked to changes in the sign and pattern of temperature bias between the low- and high-top models, as evidenced in Fig. 3. This amounts to a reduction in strength of the northern polar night jet in the high-top model of around 10 m s^{-1} at 10 hPa . Another key difference between low-top and high-top models includes strong features in the tropical stratosphere. Weak negative biases occur

FIG. 4. Same as Fig. 3, but for zonal mean zonal wind anomalies (m s^{-1}).

throughout the tropical stratosphere in the low-top model and relate to a climatological background of easterly winds. These peak in the tropical lower stratosphere, and are consistent with the absence of a quasi-biennial oscillation. This represents a clear improvement in the high-top ensemble.

Further wind biases include strong tropical easterlies near the stratopause (1 hPa), a feature not only linked with previous configurations of the Met Office high-top model (Hardiman et al. 2010; Osprey et al. 2010), but also a number of chemistry climate models (Butchart et al. 2011). This bias has been linked with a weak annual cycle and too strong semiannual oscillation (SAO).

Finally, both low-top and high-top ensembles display similar climatological features in the troposphere. Furthermore, both ensemble sets show good agreement with ERA-40 and ERA-Interim, with only minor significant differences ($\pm 5 \text{ m s}^{-1}$; 5%). A more complete analysis of tropospheric climate and variability in the low-top and high-top ensembles can be found in Hardiman et al. (2012).

b. Tropical variability

The time series of tropical zonal mean zonal wind is seen in Fig. 5. It is clearly apparent that a QBO is present

in the high-top historical simulation and absent in the low-top simulations. Climatological easterly winds and the vestige of an SAO (likely associated with the advection of summertime easterlies) replaces the QBO in the low-top times series of zonal wind in the stratosphere. The period of the QBO in the high-top simulations (27.6 months) shows very good agreement with the reanalyses (28.3 months), over the period 1960–2006. The strength of the westerly phase in the high-top time series shows a positive bias over the reanalyses at 10 hPa, though in the lowermost stratosphere the agreement is good. The strength of the easterly phase shows greater agreement with reanalyses and is discernible in the lowermost stratosphere. The easterly phase also shows occasional signs of stalling between 30 and 50 hPa, behavior thought to be linked with synchronization with the annual cycle, although this occurs less frequently than in ERA-40 (Baldwin et al. 2001; Gray and Dunkerton 1990; Wang et al. 1995).

Upwelling occurs within the tropical stratosphere because of wave-driving processes throughout the year, especially Rossby waves during winter. This mechanism constitutes the Brewer–Dobson circulation, which is important for the transport of heat and trace species, such as ozone, from low to high latitudes (Brewer 1949;

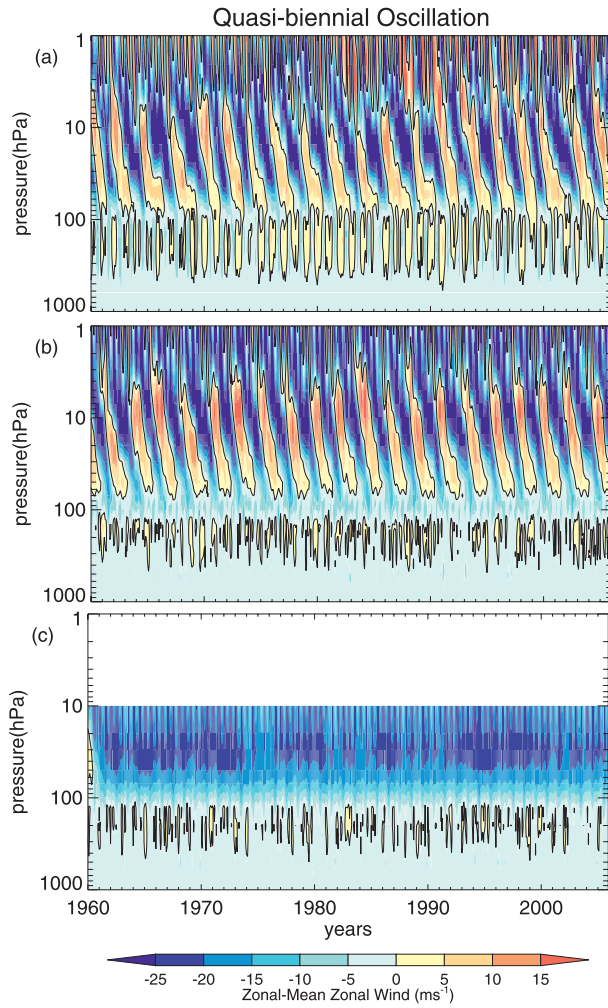


FIG. 5. Zonal mean zonal wind (m s^{-1}) between 10°S and 10°N from the (a) ERA-40 and ERA-Interim datasets, and representative (b) high-top and (c) low-top runs.

Holton et al. 1995). Two metrics quantifying the action of waves on the resolved circulation are encapsulated by meridional (\bar{v}^*) and vertical (\bar{w}^*) components of the transformed Eulerian mean (TEM) circulation, the latter being expressed as

$$\bar{w}^* \equiv \bar{w} - \frac{1}{a \cos \phi} \left(\frac{\cos \phi \bar{v}' \theta'}{\bar{\theta}_z} \right)_\phi, \quad (3)$$

where terms are defined as in Andrews et al. (1987). Figure 6 shows the TEM vertical velocity at 70 hPa as a function of latitude. The reanalyses, low-top, and high-top simulations lend support to the canonical stratospheric transport of upwelling in the tropics and downwelling at high latitudes, conserving mass. The low-top \bar{w}^* shows positive bias at low latitudes, which is

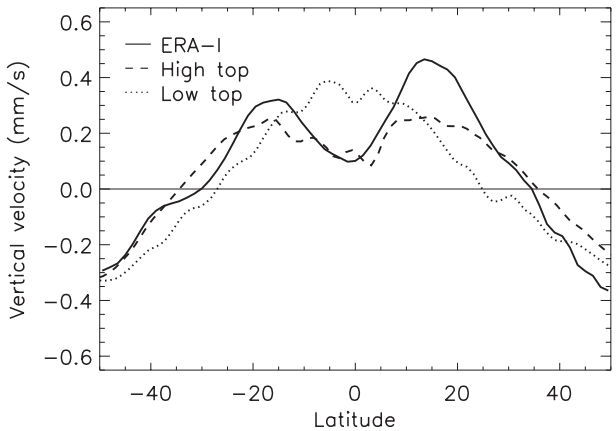


FIG. 6. Residual mean vertical velocity (mm s^{-1}) diagnosed at 70 hPa from the high-top and low-top ensembles and ERA-Interim. Note the reduced upwelling in the high-top model and ERA-Interim data at the equator.

consistent with an absence of QBO-induced circulations in the low-top simulations. The QBO would impact the propagation of large-scale Rossby waves into the stratosphere and high latitudes from lower in the troposphere. The presence of two maxima in the ERA-Interim data is not found in the ERA-40 dataset (P. Berrisford 2012, personal communication). This may suggest that the transport and radiative impact of ozone is better captured in the updated reanalyses dataset. At higher latitudes, the low-top model shows a negative bias, while the high-top model compares more favorably with reanalyses.

Differences in the tropical stratospheric circulation between high top and low top is further diagnosed using the changing concentration of water vapor. This is understood to be influenced by the temperature of the tropical tropopause, the strength of the Brewer–Dobson circulation, and irreversible horizontal mixing with higher latitudes. Collectively, this phenomenon is known to be related to the tropical tape recorder (TTR) in water vapor, evident near the tropical tropopause (Mote et al. 1996). Figure 7 shows the zonal mean, monthly mean water vapor volume-mixing ratio averaged over 20°S – 20°N for high-top and low-top simulations, and the Halogen Occultation Experiment instrument (HALOE) onboard the *Upper Atmosphere Research Satellite* (*UARS*) (Rosenlof and Reid 2008; Russell et al. 1993). One feature common to high-top and low-top simulations is the NH winter timing of minimum concentrations above the tropical tropopause. This is thought to be linked with the north–south asymmetry in the strength of the Brewer–Dobson circulation—stronger upwelling during NH winter is thought to be driven by breaking Rossby waves at midlatitudes. One other conspicuous feature of the TTR is the propagation of anomalies upward. The

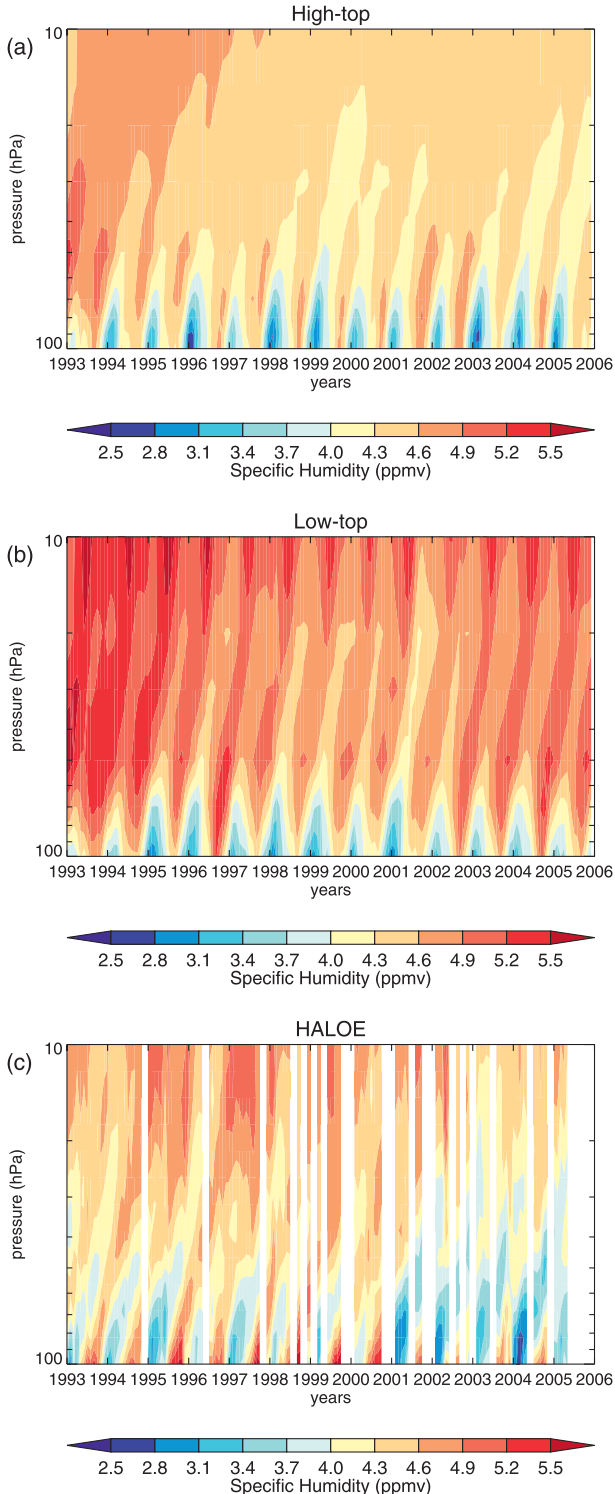


FIG. 7. Monthly mean water vapor volume mixing ratio (ppmv) in the (a) high-top and (b) low-top simulations, and (c) HALOE data between 100 and 10 hPa and 20°S and 20°N.

rate of ascent of these anomalies is a direct consequence of mean upwelling due to the Brewer–Dobson circulation. Comparisons of the ascent rate of stratospheric water vapor between low-top and high-top simulations show differences consistent with those diagnosed from \bar{w}^* (Fig. 6): stronger upwelling in the low-top simulations corresponds to a more rapid ascent rate of water vapor. Tropopause water vapor anomalies in the low-top simulations reach 32 km (10 hPa) within 12 months and would appear to be phase-locked with the annual cycle. No such phase-locking with the annual cycle is seen in the high-top simulations. The ascent rate of the latter is more consistent with HALOE data. The low-top TTR signal is consistent with the proximity of the uppermost model level (adjacent to the level near 32 km), giving rise to nonphysical meridional circulation, as vertical velocities are constrained to be identically zero there. A second difference between the low-top and high-top ensemble is the higher mean concentration seen above the cold-point tropopause in the low-top model. Once more, this is likely linked with increased horizontal mixing associated with a strengthened Brewer–Dobson circulation, mixing higher water vapor concentrations from the extratropics. The differences seen in the mean concentrations between the low-top and high-top simulations are less likely a response to differences in the temperature of the cold-point tropopause, as is evidenced by the relative temperatures and specific humidity at 100 hPa in Fig. 8. This shows little significant (5%) difference between low-top and high-top models during those times of year when water vapor near the tropopause is at a maximum or minimum.

Figure 9 shows the trend in the width in latitude of the tropical upper troposphere, following Seidel et al. (2008). This widening will be associated with a poleward shift of the midlatitude jet streams and thus expansion of the Hadley circulation (Hu and Fu 2007). Around a 2° widening in 25 yr is seen in both models, in agreement with observations as shown by the trend lines. Such good agreement is seen in only 3% of the climate models analyzed by Seidel et al. (2008). The low values seen in 1982/83 and 1991/92 are likely due to diabatic heating effects from the eruptions of El Chichón and Pinatubo. Thus the time series for high- and low-top models are well correlated.

c. Extratropical variability

The stratospheric age of air is defined as the time since that air was last in contact with the troposphere. It gives a good indication of transport throughout the stratosphere, important for the distribution of chemical species and for the thermal structure of the stratosphere. From Fig. 10 it can be seen that the age of air in the high-top

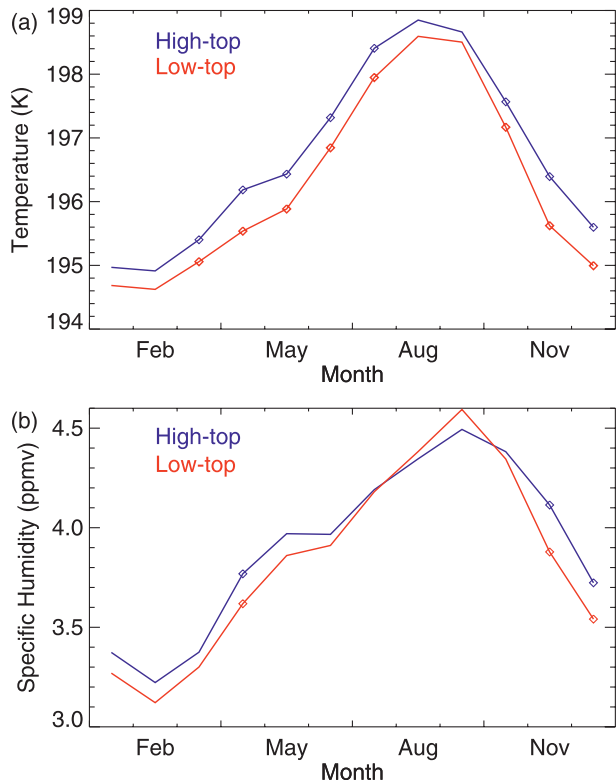


FIG. 8. Climatological zonal mean monthly mean (a) temperature (K) and (b) water vapor volume mixing ratio (ppmv) at 100 hPa and averaged between 20°S and 20°N. Symbols denote differences significant at the 95% level. Tick intervals denote month.

model is in reasonable agreement with the limited observations, but that the age of air in the low-top model is far too young (Martin et al. 2011). Likely reasons for the young age in the low-top model are too much tropical upwelling, driven by too much planetary wave breaking there (not shown), and possibly incorrect climatological stratospheric jet strengths driving a Brewer–Dobson circulation that is too deep, bringing young air to higher altitudes (E. Gerber 2012, personal communication). Thus, in the case of the Met Office Unified Model, a well-resolved stratosphere is necessary to correctly simulate stratospheric transport.

Around springtime, the stratospheric polar vortex undergoes a “final warming,” defined here as the final time over the extended winter period that zonal mean zonal wind at 60° and 10 hPa becomes easterly. The final warming in the Southern Hemisphere occurs first in the mesosphere and propagates down through the stratosphere. However, the final warming in the Northern Hemisphere occurs first in the midstratosphere (Hardiman et al. 2010). The interannual variability in the profile of the final warming has implications for surface climate

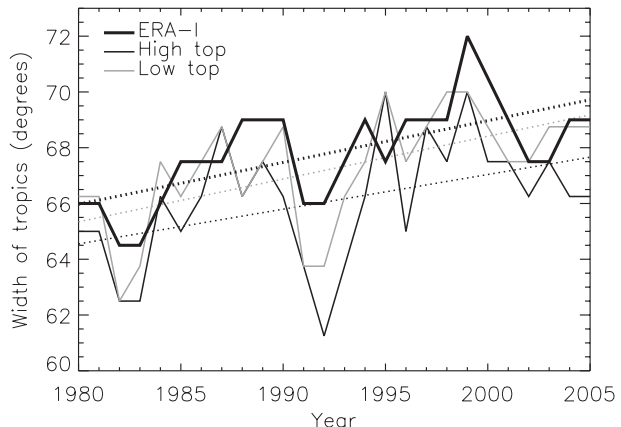


FIG. 9. Width of tropics, measured as width of latitudes (degrees) where cold-point tropopause is above 15 km for more than 100 days in the year, for ERA-Interim, high-top, and low-top models. Trend lines are also added.

(Hardiman et al. 2011) and thus it is of interest that the model can correctly simulate this profile. Figure 11 shows the final warming date for high- and low-top models and ERA-Interim. Apart from the climatological final warming occurring a few days too early, the high-top model simulates the structure and variability of the final warming very accurately. The warming occurs first in the midstratosphere, and latest at around 1 hPa, with scaled interannual standard error of around 20 days, as seen in the reanalyses. In contrast, the low-top model does not extend high enough—with the top boundary at 3 hPa—to capture this profile, and the scaled interannual standard error of the warming date is too small. Thus, a high-top model is required to simulate this aspect of extratropical variability.

When considering the effects of vertical resolution on stratospheric climate and variability, of immediate relevance are changes in the occurrence frequency of sudden stratospheric warmings. These represent one aspect of the spectrum of variability relevant to the Brewer–Dobson circulation. Figure 12 shows the occurrence of SSWs as a function of month during the historical period for ERA-40, the low-top, and the high-top simulations. The criteria for the identification and statistical analysis of these events are detailed in Charlton and Polvani (2007). The frequency of SSWs over the period 1960–2002 for ERA-40 is (6.0 ± 1.0) decade $^{-1}$. For the high-top ensemble during this period, the frequency is greater at (7.2 ± 0.5) decade $^{-1}$. Furthermore, there is a systematic bias in SSWs occurring in late winter (February–March), with a frequency double that in ERA-40. For the low-top ensemble, the bias is low, with there being a frequency of (2.5 ± 0.5) decade $^{-1}$. There is a similar trend in late winter SSWs (February–March), but with reduced

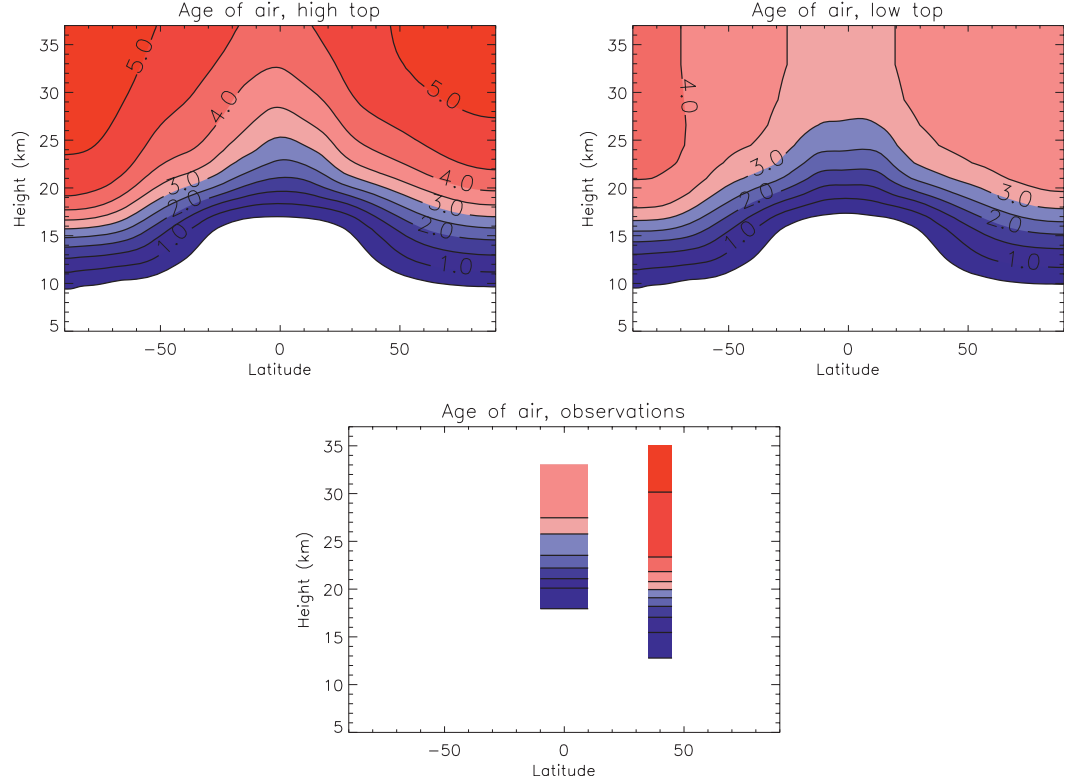


FIG. 10. Stratospheric age of air. (top left) High-top model, (top right) low-top model, and (bottom) tropical observations from Andrews et al. (2001) and subtropical observations from Engel et al. (2009).

values compared to that seen in ERA-40. In comparison with the 16 high-top chemistry climate models described in Butchart et al. (2011), the high-top model in this study just falls within the 95% confidence level compared with ERA-40. The low-top model does not.

4. Discussion and conclusions

In this study we compare the stratospheric variability diagnosed in low-top and high-top configurations of the Met Office global climate model (HadGEM2) under

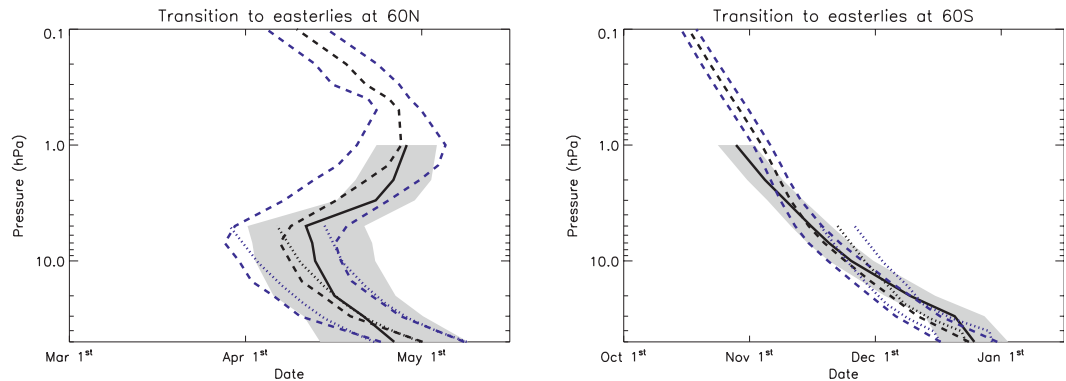


FIG. 11. (left) NH and (right) SH climatological mean final warming time, defined for each extended winter period as the final transition from westerly to easterly zonal mean flow at 60°N (S) and then averaged over 1960–2005 for high-top and low-top ensembles and 1989–2009 for ERA-Interim. Solid line shows final warming time for ERA-Interim, with shading showing the interannual standard deviation in warming time, scaled to represent a 95% confidence interval. Dashed/dotted black lines show final warming time for high/low-top model, with blue lines showing the scaled interannual standard deviation.

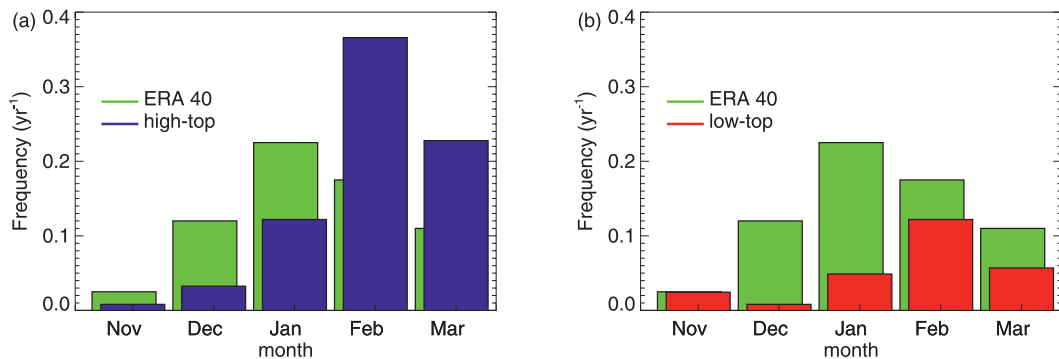


FIG. 12. NH wintertime frequency of SSW (events per year) between the (a) high-top ensemble, (b) low-top ensemble, and ERA-40.

historical forcing conditions prescribed for CMIP5. Our emphasis is on variability relating to the tropical stratosphere and extreme events occurring in the NH winter, so we restrict our conclusions to those.

The relative rates of recent surface warming are equally reproduced in low-top and high-top models. These amount to a warming post-1960 of about 0.8 K, which is consistent with HadCRUT reconstructions of global temperature (1.0 K). A notable difference between the models and observations is a lack of a secular trend in global temperature pre-1960, although sizeable decadal variability is apparent in the model. In the stratosphere, global cooling is evident in the latter part of the twentieth century, in agreement with ERA-40. Although the timing of volcanic eruptions is prescribed, only the magnitude of their effects in the postsatellite era (El Chichón, Pinatubo) agrees well with ERA-40. This perhaps suggests a limited usefulness of reanalyses in studying the stratospheric impact of past volcanic eruptions.

The low-top and high-top configurations of HadGEM2 show weak negative biases in the troposphere northward of 60°S during DJF and at low–midlatitudes during JJA. Wintertime cold biases in the extratropical stratosphere in the low-top ensemble have been largely alleviated in the high-top ensemble. This is less likely due to small-scale gravity wave forcing than due to circulation changes following the dissipation of Rossby waves. These circulation changes are also seen in zonal mean zonal wind and show up as a weakened polar night jet and are more consistent with ERA-40 and ERA-Interim during NH winter. A negative bias in zonal mean zonal wind about the tropical stratopause, which has been linked with a weak annual cycle, is also present in the high-top ensemble.

Significant differences are seen in tropical variability between low-top and high-top ensembles and a combination of ERA-40, ERA-Interim, and HALOE observations. The main anomaly is the lack of a QBO in the low-top ensemble, but that is present in the high-top

ensemble. Associated with this are differences in mean tropical upwelling, diagnosed by the vertical component of the TEM residual mean circulation. The tropical upwelling in the low-top ensemble is around twice the strength as compared with the high-top ensemble and ERA-Interim (though not ERA-40). These differences are also seen in the rate of ascent of the TTR, which implies a 50% stronger upwelling in the low-top ensemble. The relative rate of horizontal mixing as diagnosed from calculations for the age of air is also greater in the low-top ensemble. This is inferred from a reduced horizontal gradient in age of air in the extratropical stratosphere of the low-top ensemble. In the high-top ensemble, the magnitude, vertical, and horizontal gradients of this are more consistent with what little observations there are at this time. Finally, a sensitivity of the width of the tropics to volcanic eruptions is reproduced in both configurations of HadGEM2, consistent with ERA-40. There do not appear to be any statistically discernible trends in the latter half of the twentieth century.

The variability of the wintertime extratropical vortex is mediated by the presence and dissipation of Rossby waves. The dissipation of these waves can result in extended periods when the stratospheric jet is weak, bringing forward the timing of the final warming. The vertical profile of final warming times is qualitatively different between SH and NH. The SH shows a cessation of winter westerlies starting in the upper atmosphere. The NH timings show the cessation of wintertime westerlies starting around 7 hPa and a delay near 1 hPa. This latter feature, by construction, is absent in the low-top ensemble. Furthermore, the rates and seasonality of SSWs are very different between low-top and high-top ensembles. Although the model shows a consistent bias toward late winter SSWs, the relative rates are much reduced in the low-top ensemble.

We have shown large differences between the two model configurations, which suggests that adequate representation

of stratospheric variability requires explicit resolution of the stratosphere. Although large and significant differences are seen in stratospheric climatology, variability, and circulation, it is not immediately obvious what impact greater vertical resolution has on reproducing global changes in temperature and perhaps consequently, climate sensitivity. Future work will necessarily require a closer examination of stratospheric variability and its possible feedback on changing tropospheric climate into the twenty-first century.

Acknowledgments. The authors thank the whole of the HadGEM2 team at the Met Office. We are also especially grateful to Sean Davis for helpful comments and suggestions. S. Osprey and L. Gray were supported by the NERC National Centre for Atmospheric Science (NCAS) Climate directorate, while N. Butchart and S. C. Hardiman were supported by the Joint DECC and Defra Integrated Climate Programme (DECC/Defra GA01101).

REFERENCES

- Andrews, A. E., and Coauthors, 2001: Mean ages of stratospheric air derived from in situ observations of CO₂, CH₄, and N₂O. *J. Geophys. Res.*, **106** (D23), 32 295–32 314.
- Andrews, D. G., J. R. Holton, and C. B. Leovy, 1987: *Middle Atmosphere Dynamics*. International Geophysical Series, Vol. 40, Academic Press, 489 pp.
- Baldwin, M. P., and T. J. Dunkerton, 2001: Stratospheric harbingers of anomalous weather regimes. *Science*, **294**, 581–584, doi:10.1126/science.1063315.
- , and Coauthors, 2001: The quasi-biennial oscillation. *Rev. Geophys.*, **39**, 179–229.
- , D. B. Stephenson, D. W. J. Thompson, T. J. Dunkerton, A. J. Charlton, and A. O'Neill, 2003: Stratospheric memory and skill of extended-range weather forecasts. *Science*, **301**, 636–640, doi:10.1126/science.1087143.
- Bell, C. J., L. J. Gray, A. J. Charlton-Perez, M. M. Joshi, and A. A. Scaife, 2009: Stratospheric communication of El Niño teleconnections to European winter. *J. Climate*, **22**, 4083–4096.
- Brewer, A. W., 1949: Evidence for a world circulation provided by the measurements of helium and water vapour distribution in the stratosphere. *Quart. J. Roy. Meteor. Soc.*, **75**, 351–363, doi:10.1002/qj.49707532603.
- Brohan, P., J. J. Kennedy, I. Harris, S. F. B. Tett, and P. D. Jones, 2006: Uncertainty estimates in regional and global observed temperature changes: A new data set from 1850. *J. Geophys. Res.*, **111**, D12106, doi:10.1029/2005JD006548.
- Butchart, N., and Coauthors, 2011: Multimodel climate and variability of the stratosphere. *J. Geophys. Res.*, **116**, D05102, doi:10.1029/2010JD014995.
- Charlton, A. J., and L. M. Polvani, 2007: A new look at stratospheric sudden warmings. Part I: Climatology and modeling benchmarks. *J. Climate*, **20**, 449–469.
- Cionni, I., and Coauthors, 2011: Ozone database in support of CMIP5 simulations: Results and corresponding radiative forcing. *Atmos. Chem. Phys. Discuss.*, **11**, 10 875–10 933, doi:10.5194/acpd-11-10875-2011.
- Cox, P. M., R. A. Betts, C. D. Jones, S. A. Spall, and I. J. Totterdell, 2000: Acceleration of global warming due to carbon-cycle feedbacks in a coupled climate model. *Nature*, **408**, 184–187, doi:10.1038/35041539.
- Dall'Amico, M., P. A. Stott, A. A. Scaife, L. J. Gray, K. H. Rosenlof, and A. Y. Karpechko, 2010: Impact of stratospheric variability on tropospheric climate change. *Climate Dyn.*, **34** (2–3), 399–417, doi:10.1007/s00382-009-0580-1.
- Dee, D. P., and Coauthors, 2011: The ERA-Interim reanalysis: Configuration and performance of the data assimilation system. *Quart. J. Roy. Meteor. Soc.*, **137**, 553–597, doi:10.1002/qj.828.
- Engel, A., and Coauthors, 2009: Age of stratospheric air unchanged within uncertainties over the past 30 years. *Nat. Geosci.*, **2**, 28–31, doi:10.1038/NGEO388.
- Gray, L., and T. Dunkerton, 1990: The role of the seasonal cycle in the quasi-biennial oscillation of ozone. *J. Atmos. Sci.*, **47**, 2429–2451.
- Hardiman, S. C., N. Butchart, S. M. Osprey, L. J. Gray, A. C. Bushell, and T. J. Hinton, 2010: The climatology of the middle atmosphere in a vertically extended version of the Met Office's climate model. Part I: Mean state. *J. Atmos. Sci.*, **67**, 1509–1525.
- , and Coauthors, 2011: Improved predictability of the troposphere using stratospheric final warmings. *J. Geophys. Res.*, **116**, D18113, doi:10.1029/2011JD015914.
- , N. Butchart, T. J. Hinton, S. M. Osprey, and L. J. Gray, 2012: The effect of a well-resolved stratosphere on surface climate: Differences between CMIP5 simulations with high and low top versions of the Met Office Climate Model. *J. Climate*, **25**, 7083–7099.
- Holton, J., P. Haynes, M. McIntyre, A. Douglass, R. Rood, and L. Pfister, 1995: Stratosphere-troposphere exchange. *Rev. Geophys.*, **33**, 403–439.
- Hu, Y., and Q. Fu, 2007: Observed poleward expansion of the Hadley circulation since 1979. *Atmos. Chem. Phys.*, **7**, 5229–5236.
- Ineson, S., and A. A. Scaife, 2009: The role of the stratosphere in the European climate response to El Niño. *Nat. Geosci.*, **2**, 32–36, doi:10.1038/ngeo381.
- Jones, C. D., and Coauthors, 2011: HadGEM2-ES implementation of CMIP5 centennial simulations. *Geosci. Model Dev.*, **4**, 543–570, doi:10.5194/gmd-4-543-2011.
- Jones, P., and A. Moberg, 2003: Hemispheric and large-scale surface air temperature variations: An extensive revision and an update to 2001. *J. Climate*, **16**, 206–223.
- , M. New, D. Parker, S. Martin, and I. Rigor, 1999: Surface air temperature and its changes over the past 150 years. *Rev. Geophys.*, **37**, 173–199.
- Martin, G. M., and Coauthors, 2011: The HadGEM2 family of Met Office Unified Model Climate configurations. *Geosci. Model Dev. Discuss.*, **4**, 765–841, doi:10.5194/gmdd-4-765-2011.
- Martius, O., L. M. Polvani, and H. C. Davies, 2009: Blocking precursors to stratospheric sudden warming events. *Geophys. Res. Lett.*, **36**, L14806, doi:10.1029/2009GL038776.
- Maycock, A. C., S. P. E. Keeley, A. J. Charlton-Perez, and F. J. Doblas-Reyes, 2011: Stratospheric circulation in seasonal forecasting models: Implications for seasonal prediction. *Climate Dyn.*, **36** (1–2), 309–321, doi:10.1007/s00382-009-0665-x.
- Mitchell, J. F. B., T. C. Johns, J. M. Gregory, and S. F. B. Tett, 1995: Climate response to increasing levels of greenhouse gases and sulfate aerosols. *Nature*, **376**, 501–504, doi:10.1038/376501a0.

- Mote, P. W., and Coauthors, 1996: An atmospheric tape recorder: The imprint of tropical tropopause temperatures on stratospheric water vapor. *J. Geophys. Res.*, **101** (D2), 3989–4006.
- Norton, W. A., 2003: Sensitivity of northern hemisphere surface climate to simulation of the stratospheric polar vortex. *Geophys. Res. Lett.*, **30**, 1627, doi:10.1029/2003GL016958.
- Osprey, S. M., L. J. Gray, S. C. Hardiman, N. Butchart, A. C. Bushell, and T. J. Hinton, 2010: The climatology of the middle atmosphere in a vertically extended version of the Met Office's climate model. Part II: Variability. *J. Atmos. Sci.*, **67**, 3637–3651.
- Quiroz, R. S., 1986: The association of stratospheric warmings with tropospheric blocking. *J. Geophys. Res.*, **91** (D4), 5277–5285.
- Rayner, N. A., D. E. Parker, E. B. Horton, C. K. Folland, L. V. Alexander, D. P. Rowell, E. C. Kent, and A. Kaplan, 2003: Global analyses of sea surface temperature, sea ice, and night marine air temperature since the late nineteenth century. *J. Geophys. Res.*, **108**, 4407, doi:10.1029/2002JD002670.
- , P. Brohan, D. E. Parker, C. K. Folland, J. J. Kennedy, M. Vanicek, T. J. Ansell, and S. F. B. Tett, 2006: Improved analyses of changes and uncertainties in sea surface temperature measured in situ since the mid-nineteenth century: The HadSST2 dataset. *J. Climate*, **19**, 446–469.
- Roeckner, E., L. Bengtsson, J. Feichter, J. Lelieveld, and H. Rodhe, 1999: Transient climate change simulations with a coupled atmosphere–ocean GCM including the tropospheric sulfur cycle. *J. Climate*, **12**, 3004–3032.
- Rosenlof, K. H., and G. C. Reid, 2008: Trends in the temperature and water vapor content of the tropical lower stratosphere: Sea surface connection. *J. Geophys. Res.*, **113**, D06107, doi:10.1029/2007JD009109.
- Russell, J. M., III, and Coauthors, 1993: The Halogen Occultation Experiment. *J. Geophys. Res.*, **98** (D6), 10 777–10 797.
- Sassi, F., R. R. Garcia, D. Marsh, and K. W. Hoppel, 2010: The role of the middle atmosphere in simulations of the troposphere during Northern Hemisphere winter: Differences between high- and low-top models. *J. Atmos. Sci.*, **67**, 3048–3064.
- Scaife, A., N. Butchart, C. Warner, and R. Swinbank, 2002: Impact of a spectral gravity wave parameterization on the stratosphere in the Met Office Unified Model. *J. Atmos. Sci.*, **59**, 1473–1489.
- , J. R. Knight, G. K. Vallis, and C. K. Folland, 2005: A stratospheric influence on the winter NAO and North Atlantic surface climate. *Geophys. Res. Lett.*, **32**, L18715, doi:10.1029/2005GL023226.
- , and Coauthors, 2012: Climate change projections and stratosphere–troposphere interaction. *Climate Dyn.*, **38** (9–10), 2089–2097, doi:10.1007/s00382-011-1080-7.
- Seidel, D. J., Q. Fu, W. J. Randel, and T. J. Reichler, 2008: Widening of the tropical belt in a changing climate. *Nat. Geosci.*, **1**, 21–24, doi:10.1038/ngeo.2007.38.
- , N. P. Gillett, J. R. Lanzante, K. P. Shine, and P. W. Thorne, 2011: Stratospheric temperature trends: Our evolving understanding. *Wiley Interdiscip. Rev.: Climate Change*, **2**, 592–616, doi:10.1002/wcc.125.
- Shaw, T. A., and T. G. Shepherd, 2008: Atmospheric science: Raising the roof. *Nat. Geosci.*, **1**, 12–13, doi:10.1038/ngeo.2007.53.
- Sigmond, M., J. F. Scinocca, and P. J. Kushner, 2008: Impact of the stratosphere on tropospheric climate change. *Geophys. Res. Lett.*, **35**, L12706, doi:10.1029/2008GL033573.
- Simmons, A. J., A. Untch, C. Jakob, P. Kallberg, and P. Uden, 1999: Stratospheric water vapour and tropical tropopause temperatures in ECMWF analyses and multi-year simulations. *Quart. J. Roy. Meteor. Soc.*, **125**, 353–386, doi:10.1256/smsqj.55316.
- Solomon, S., D. Qin, M. Manning, M. Marquis, K. Averyt, M. M. B. Tignor, H. L. Miller Jr., and Z. Chen, Eds., 2007: *Climate Change 2007: The Physical Science Basis*. Cambridge University Press, 996 pp.
- Stott, P. A., S. F. B. Tett, G. S. Jones, M. R. Allen, J. F. B. Mitchell, and G. J. Jenkins, 2000: External control of 20th century temperature by natural and anthropogenic forcings. *Science*, **290**, 2133–2137, doi:10.1126/science.290.5499.2133.
- Taguchi, M., 2008: Is there a statistical connection between stratospheric sudden warming and tropospheric blocking events? *J. Atmos. Sci.*, **65**, 1442–1454.
- Uppala, S. M., and Coauthors, 2005: The ERA-40 Re-Analysis. *Quart. J. Roy. Meteor. Soc.*, **131**, 2961–3012, doi:10.1256/qj.04.176.
- Wang, R., K. Fraedrich, and S. Pawson, 1995: Phase–space characteristics of the tropical stratospheric quasi-biennial oscillation. *J. Atmos. Sci.*, **52**, 4482–4500.
- Woollings, T., A. Charlton-Perez, S. Ineson, A. G. Marshall, and G. Masato, 2010a: Associations between stratospheric variability and tropospheric blocking. *J. Geophys. Res.*, **115**, D06108, doi:10.1029/2009JD012742.
- , M. Lockwood, G. Masato, C. Bell, and L. Gray, 2010b: Enhanced signature of solar variability in Eurasian winter climate. *Geophys. Res. Lett.*, **37**, L20805, doi:10.1029/2010GL044601.
- Zhong, W., and J. D. Haigh, 2000: An efficient and accurate correlated-k parameterization of infrared radiative transfer for troposphere–stratosphere–mesosphere GCMs. *Atmos. Sci. Lett.*, **1**, 125–135, doi:10.1006/asle.2000.0014.